# Multiple Equilibrium Analysis Description of Adsorption on Na−Mordenite and H−Mordenite

**Charles Edwin Webster,* Andrew Cottone, III, and Russell S. Drago†**

*Contribution from the Center for Catalysis, Department of Chemistry, P.O. Box 117200, University of Florida, Gainesville, Florida 32611-7200*

*Received November 30, 1998. Revised Manuscript Received August 6, 1999*

**Abstract:** Adsorption isotherms are reported for Na−mordenite and H−mordenite at several temperatures with a series of gas adsorptives above their critical temperature. The data sets are analyzed with the multiple equilibrium analysis (MEA) method [Drago, R. S.; et al. *J. Am. Chem. Soc.* **1998**, *120*, 538−547. Drago, R. S.; et al. *J. Phys. Chem. B* **1997**, *101*, 7548−7555], which produces equilibrium constants ($K_i$), capacities ($n_i$), and thermodynamic parameters (enthalpies, $\Delta H_i$, and entropies, $\Delta S_i$) of adsorption for each process. The limited pore size distribution present in the zeolite mordenite presents an interesting comparison to the amorphous carbons studied previously by MEA [Drago, R. S.; et al. *J. Phys. Chem. B* **1997**, *101*, 7548−7555]. The results of the MEA description of the adsorption data gathered for the interaction of an adsorbate (particularly, $N_2$, CO, and Xe) with Na−mordenite and H−mordenite are compared to other literature reports (including infrared spectroscopic studies and Monte Carlo simulations), and good agreement is found. In general, for adsorbates that can access the small channel (small adsorbates), three processes are required to describe adsorption. Two processes are required to describe adsorption for the larger adsorbates into the large (main) channel. The smaller total micropore volumes of Na− and H−mordenite for these adsorptives result in decreased capacity compared to that of the amorphous carbons. The process capacities from MEA (mol $g^{-1}$) are converted to pore volumes using the calculated molar volume of the adsorbate, and the accessible surface area for a given process is converted with the excluded molecular area of the adsorbate. The results show that MEA provides a more detailed and accurate assessment of the interaction of admolecules with microporous solids, which addresses a matter of fundamental importance to researchers and practitioners—the interactions between gas-phase molecules and a surface of a condensed phase. This analysis leads to an increased understanding of this behavior in gas adsorption and catalysis.

## Introduction

Gas adsorption of a given adsorbate, $A_{(g)}$, by a solid adsorbent, $S_{(s)}$, is described by eq 1, where $SA_{(s)}$ is the total amount of

$$S_{(s)} + A_{(g)} \rightleftharpoons SA_{(s)} \tag{1}$$

$A_{(g)}$ adsorbed per gram of solid. Rearrangement of the thermodynamic equilibrium expression describing eq 1, assuming homogeneous energetic adsorption interactions, yields eq 2,[1,2] where $n$ is the capacity of the solid for adsorption, $K$ is the

$$[SA]_s = \frac{nK[P]}{1 + K[P]} \tag{2}$$

equilibrium constant, and $P$ is the equilibrium pressure. Although eq 2 is similar in form to the Langmuir equation,[3] the distribution type equilibrium constant ($K$) refers to a process, not a specific, isolated binding site on a planar surface. The conceptual basis of this process equilibrium analysis eliminates the assumptions required[2] to apply the Langmuir model to binding at a solid site.

As demonstrated in the first five papers of this series,[4] multiple adsorption processes are required to adequately describe a system with heterogeneous energetic interactions, such as porous carbonaceous materials or zeolites (HZSM-5 and TS-1). The expansion of eq 2 to include multiple processes yields eq 3, where $n_i$ is the capacity of the solid for adsorption for the

$$[SA]_s = \sum_{i=1}^{i} \frac{n_i K_i[P]}{1 + K_i[P]} \tag{3}$$

$i$th process and $K_i$ is the equilibrium constant for the $i$th process. This expression is employed in the multiple equilibrium analysis (MEA) of gas−solid interactions.[4]

An innovation of the MEA model is the resolution of adsorbate interactions with homogeneous regions of a heterogeneous solid and the definition of the $n_i$ and $K_i$ of these processes. This information is gathered through the measurement of adsorption isotherms at multiple temperatures measured above

* To whom correspondence should be addressed. Tel.: (352) 392-5263. Fax: (352) 392-4658.

† Deceased, Dec 5, 1997.

(1) Gregg, S. J.; Sing, K. S. W. *Adsorption, Surface Area and Porosity*, 2nd ed.; Academic Press: London, 1982 **(**and references therein).

(2) Adamson, A. W. *Physical Chemistry of Surfaces*, 5th ed.; John Wiley & Sons, Inc.: New York, 1990.

(3) Langmuir, I. *J. Am. Chem. Soc.* **1918**, *40*, 1361−1403.

(4) (a) Drago, R. S.; Burns, D. S.; Lafrenz, T. J. *J. Phys. Chem.* **1996**, *100*, 1718−1724. (b) Drago, R. S.; Kassel, W. S.; Burns, D. S.; McGilvray, J. M.; Lafrenz, T. J.; Showalter, S. K. *J. Phys. Chem. B* **1997**, *101*, 7548−7555. (c) Kassel, W. S.; Drago, R. S. *Microporous Mater.* **1997**, *12*, 189−195. (d) Drago, R. S.; Webster, C. E.; McGilvray, J. M. *J. Am. Chem. Soc.* **1998**, *120*, 538−547. (e) Drago, R. S.; Dias, S. C.; McGilvray, J. M.; Mateus, A. *J. Phys. Chem. B* **1998**, *102*, 1508−1514.

10.1021/ja984122r CCC: $18.00 
Published on Web 12/14/1999

the critical temperature ($T_c$) of the adsorbate. The process capacities ($n_i$) are a characteristic of the solid and do not change with temperature, while the equilibrium constant ($K_i$) is temperature dependent. The resolvability of the different adsorbate−adsorbent interactions at a given temperature leads to the definition of processes. A process is defined by the order of pore filling; i.e., the highest magnitude $K_i$ is the first process. At equilibrium and excluding specific interactions, the first pores to fill will be those similar in size to the probe because these interactions have the most negative enthalpy and entropy of adsorption. The wide pore size distribution in amorphous solids allows for the pores used in a given process to vary with the probe size. A solid with limited pore dimensions (e.g., mordenite or ZSM-5) does not possess the versatility of pore sizes encountered in amorphous solids. Heterogeneous solids sometimes undergo reversals in the enthalpy of adsorption ($\Delta H_i$) and the order of pore filling (highest $K_i$).[4d,e] The concept of a process, alone, is not an adequate descriptor of solids with a limited pore size distribution. The description of the different interactions encountered in heterogeneous solids with crystalline frameworks (which have a limited pore size, e.g., zeolites) requires the use of new terminology—process and type designation.[4d] A type, as defined previously,[4d] is a relationship between the molecular diameter of the adsorbate and the pore width of the adsorbent. A type 1 interaction defines the interaction of a probe with pores that are closest in size to itself, i.e., a strong interaction with two opposing walls (a pore size of 1.0−1.2 molecular diameters). A type 2 interaction describes a probe adsorbed in a pore where the adsorbate is interacting strongly with one wall and weakly with the opposite (a pore size of 1.2−1.4 molecular diameters). An interaction with only one wall is the weakest, designated type 3 (a pore size greater than 1.4 molecular diameters). Considering a solid with a limited pore size distribution like mordenite, one can envision a smaller probe (e.g., $N_2$) exhibiting the maximum interaction in a different region of the framework than a larger molecule (e.g., $SF_6$) because the smaller molecule can access regions that the larger molecule cannot.

Previous MEA studies have explored the porosity of carbons,[4a−c] silica gel,[4d] and other zeolites (HZSM-5,[4d] TS-1,[4e] and H−Y[5]). These other zeolites present an interesting comparison to the straight, intersecting, elliptical channels of mordenite. For instance, the zeolite HZSM-5[6] is comprised of similar-sized straight channels (5.75 Å × 5.22 Å) and intersecting sinusoidal channels (5.55 Å × 5.29 Å).[7,8] Mordenite is comprised of two different-sized channels (see Figure 1). The larger channel, commonly referred to as the "main channel", exists parallel to the *c* axis. The free aperture to the main channel is a twelve-member oxygen ring with reported crystallographic dimensions of 6.69 Å × 7.05 Å.[9a,10] The smaller channels, often referred to as the "side-pockets", are a more complex series of offset channels that intersect the larger channel along the *b* symmetry axis. The reported crystallographic dimensions for the small channel include an eight-member oxygen ring with an aperture of 4.82 Å × 3.97 Å.[9] The crystallographically determined values for the large channel aperture have been questioned.[11] From catalytic studies, Csicsery reports the presence of various molecules in the aluminosilicate framework of H−mordenite (H−MOR) that are larger than the reported crystallographic dimensions,[11] e.g., 1,3,5-trimethylbenzene (MIN-2 of 8.3 Å) and 1,2,3-trimethylbenzene (MIN-2 of 7.9 Å), where MIN-2[12] is the second minimum dimension calculated from molecular dimensions that directly correlate with bulk molar volumes.[12] Csicsery concluded that these larger molecular species could not enter the structure if the aperture to the framework has the reported crystallographic dimensions.[11] It should be noted that zeolitic frameworks are flexible, especially at higher temperatures frequently used in catalysis. This has been discussed previously for the zeolite HZSM-5, and an "effective catalytic pore size" has been determined for HZSM-5 from a comparison of gas chromatography and MAS NMR measurements of HZSM-5 heterogeneously catalyzed reactions.[13]

Since the acidic form of mordenite (H−MOR) is often utilized in catalytic industrial processes, the complete characterization of the acidic properties is of interest. Many techniques, such as

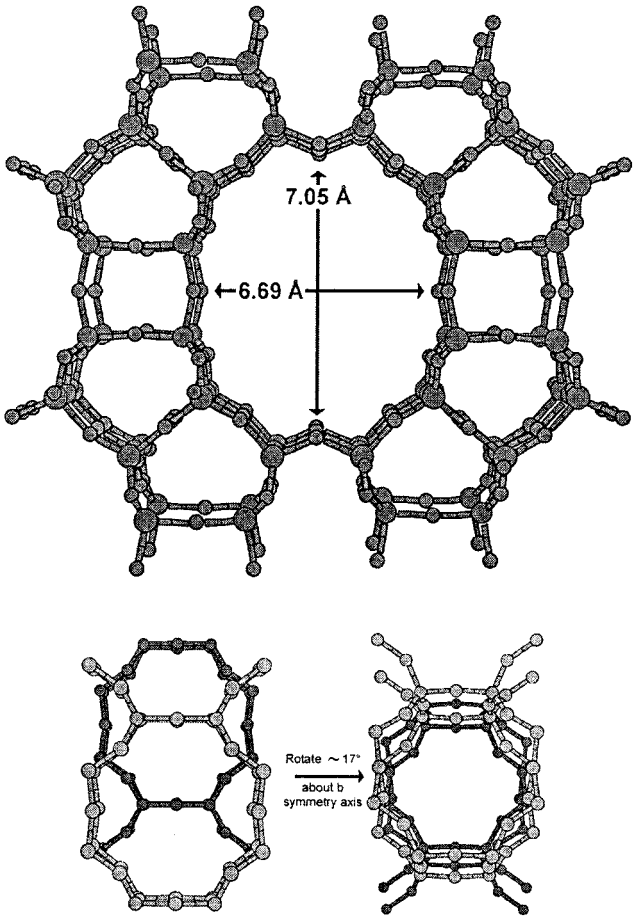


**Figure 1.** Schematic for the mordenite aluminosilicate framework. Based on fractional coordinates of ref 10a. The small channels have an opening of 4.82 Å × 3.97 Å. When the structure is rotated ~17° about the *b* symmetry axis, the free aperture between two adjacent channels is ~3.4 Å × ~4.0 Å.

(5) Dias, S. C.; Webster, C. E.; Cottone, A.; Drago, R. S. To be submitted.

(6) Breck, D. W. *Zeolite Molecular Seives*; John Wiley and Sons: New York, 1974. Chen, N. Y.; Degnan, T. F.; Smith, C. M. *Molecular Transport and Reaction in Zeolites*; VCH Publishers: New York, 1994. Jansen, J. C.; Stocker, M.; Karge, H. G.; Weitkamp, J. *Advanced Zeolite Science and Applications*; Elsevier: Amsterdam, 1994; Vol. 85.

(7) These dimensions are based on an oxygen atom radius of 1.35 Å, with the fractional coordinates of ref 8.

(8) van Koningsveld, H.; van Bekkum, H.; Jansen, J. C. *Acta Crystallogr.* **1987**, *B43*, 127−132.

(9) (a) These dimensions are based on an oxygen atom radius of 1.35 Å, with the fractional coordinates of ref 10a. (b) Since "side pockets" are offset, the opening to a small channel and the opening to the next consecutive small channel create an ~3.4 Å × ~4.0 Å "free aperture" between consecutive "side pockets" (based on an oxygen atom radius of 1.35 Å).

(10) (a) Meier, W. M. *Z. Kristallogr*. **1961**, *115*, 439−450. (b) Barrer, R. M.; White, E. A. D. *J. Chem. Soc.* **1952**, 1561−1571.

(11) Csicsery, S. M. *J. Catal.* **1971**, *23*, 124−130.

(12) Webster, C. E.; Drago, R. S.; Zerner, M. C. *J. Am. Chem. Soc.* **1998**, *120*, 5509−5516.

(13) Webster, C. E.; Drago, R. S.; Zerner, M. C. *J. Phys. Chem. B* **1999**, *103*, 1242−1249.

**Table 1.** Summary of Physical and Molecular Properties of Adsorbates

| probe gas[a] | MW (g mol$^{-1}$) | polarizability[b] (Å$^3$) | dipole moment[c] (Debye) | *MVL*[d] (mL mol$^{-1}$) | critical temp (°C) | boiling point (°C) | $\Delta H°_v$ (kcal mol$^{-1}$) | $\Delta S°_v$ (cal mol$^{-1}$ K$^{-1}$) | van der Waals const. *a* | molecular area[d] (Å$^2$) | molecular radius[d] (Å) | molecular dimens.[d] (Å) MIN-1 | MIN-2 |
|---|---|---|---|---|---|---|---|---|---|---|---|---|---|
| $O_2$ | 32.00 | 1.58 | 0 | 23.55 | −118.4 | −183.0 | 1.63 | 18.08 | 1.360 | 14.66 | 2.106 | 2.93 | 2.99 |
| $N_2$ | 28.01 | 1.74 | 0 | 25.02 | −146.9 | −195.8 | 1.332 | 17.22 | 1.390 | 15.27 | 2.149 | 2.99 | 3.05 |
| CO | 28.01 | 1.95 | 0.13 | 28.28 | −140.2 | −191.5 | 1.443 | 17.67 | 1.485 | 15.77 | 2.238 | 3.28 | 3.34 |
| Ar | 39.95 | 1.64 | 0 | 29.05 | −122.4 | −185.9 | 1.56 | 17.88 | 1.345 | 15.17 | 2.258 | 3.51 | 3.63 |
| $CH_4$ | 16.04 | 2.59 | 0 | 29.74 | −82.6 | −161.5 | 1.96 | 17.5 | 2.253 | 16.26 | 2.276 | 3.83 | 3.94 |
| Xe | 131.29 | 4.04 | 0 | 44.06 | 16.9 | −107.1 | 3.02 | 18.18 | 4.194 | 18.18 | 2.594 | 4.04 | 4.17 |
| $C_2H_6$ | 30.07 | 4.47 | 0 | 47.21 | 32.3 | −88.65[b] | 3.51 | 19.0 | 5.489 | 24.01 | 2.655 | 3.81 | 4.08 |
| $SF_6$ | 146.05 | 6.54 | 0 | 77.04 | 45.55 | $-63.8_{sub}$ | 4.08 | 19.5 | 7.365[e] | 31.17 | 3.126 | 4.87 | 5.27 |
| $C_3H_8$ | 44.1 | 6.29 | 0.084 | 64.53 | 96.7 | −42.1 | 4.54 | 19.6 | 8.664 | 28.27 | 2.946 | 4.02 | 4.52 |
| *i*-$C_4H_{10}$ | 58.12 | | 0.132 | 82.03 | 134.7 | −11.63 | 5.089 | 19.46 | 12.870 | 35.27 | 3.184 | 4.63 | 6.00 |
| *n*-$C_4H_{10}$ | 58.12 | 8.20 | <0.05 | 81.40 | 152 | −0.05 | 5.035 | 18.44 | 14.470 | 38.37 | 3.192 | 4.01 | 4.52 |

[a] *Lange's Handbook of Chemistry*, 14th ed; McGraw-Hill: New York, 1992. All data are from this source unless otherwise specified. [b] *Handbook of Chemistry and Physics*, 71st ed; CRC Press: Boca Raton, FL, 1991. [c] McClellan, A. L. *Tables of Experimental Dipole Moments*; W. H. Freeman and Co.: San Francisco, 1963. [d] Due to contradictions in the literature values, molar volumes (*MVL*), excluded molecular areas, and molecular dimensions of the adsorbates are calculated using ZINDO.[12,32] See text of ref 12 for more discussion. [e] Reference 4d, Table 2.

temperature-programmed desorption,[14] various nuclear magnetic resonance methods,[15] and infrared spectrocopy,[16] have been employed to study the interactions between a basic probe and H−MOR. Since the MEA model has the ability to characterize heterogeneous gas−solid interactions, it is interesting to explore the differences in gas adsorption between Na−mordenite (Na−MOR) and H−MOR. The analysis of the data gathered from Na−MOR and H−MOR (each with a limited pore size distribution) provides confirmation of the insights gained by the MEA model for gas adsorption.

## Experimental Section

**Gases.** The gases $CH_4$, $C_2H_6$, $C_3H_8$, *i*-$C_4H_{10}$, *n*-$C_4H_{10}$, and Xe were purchased from Matheson. $N_2$ and CO were purchased from BITEC. $O_2$ was purchased from Alphagaz, $SF_6$ was purchased from Aldrich, and Ar was purchased from AIRCO. All gases are 99.99% pure and were used as received. Pertinent physical and molecular properties of the above gases can be found in Table 1.

**Solid Preparation and Analysis.** Na−mordenite ($SiO_2/Al_2O_3$ = 39.5, Lot No. 1716-23) was donated by Zeolyst International. Prior to the adsorption experiments, the Na−MOR sample was degassed under vacuum for 8 h at 200 °C. The IR spectrum of the degassed Na−MOR demonstrated no ammonium ions or water. H−MOR was prepared by exchanging $Na^+$ for $NH_4^+$ via soaking the Na−MOR in a solution of $NH_4Cl$ (three repeated rinses) and then filtering, followed by calcining the sample under vacuum at 400 °C for ∼12 h. $NH_{3(g)}$ was released during the calcination, thereby producing H−mordenite. The resulting solid was stored under an inert atmosphere to prevent degradation from moisture. H−MOR samples were analyzed for bulk sodium content by inductively coupled plasma optical emission spectrometer (ICP-OES, Perkin-Elmer Optima 3200 RL [Radial Viewed] optical emission spectrometer) at the Engineering Research Center for Particle Science and Technology at the University of Florida. The H−MOR sample was digested by the method reported by Peru and Collins (cold digestion with a mixture of HF, HCl, $HNO_3$, and boric acid).[17] The sodium exchange for the H−MOR samples was found to be greater than 99%. The Brönsted and Lewis acidities of H−MOR were analyzed by IR spectroscopy (FT-IR Bruker Vector 22) with pyridine. IR bands at 1632, 1620, 1542, 1488, and 1390 cm$^{-1}$ were observed (indicative of Brönsted acidity) as well as bands at 1620, 1488, and 1452 cm$^{-1}$ (indicative of Lewis acidity) for the interaction of pyridine with the H−MOR samples.[16j]

**Table 2.** Physical Properties of Na−Mordenite and H−Mordenite

| | Na−Mor | H−Mor |
|---|---|---|
| surface area (m$^2$ g$^{-1}$) | | |
| MEA[a] | 265 | 346 |
| BET[b] | 458 | 462 |
| pore volume ($\mu$L g$^{-1}$) | | |
| micropore[c] | 175 | 171 |
| mesopore[d] | 97 | 88 |
| macropore[d] | – | – |

[a] MEA accessible surface area from $CH_4$ porosimetry. [b] BET surface area from $N_2$ porosimetry at 77 K.[18] [c] Micropore volume calculated from the Harkins−Jura *t*-plot model.[19] [d] Meso- and macropore volumes calculated from BJH desorption data.[20]

Using a Micromeritics ASAP 2000 gas analyzer, the Brunauer−Emmett−Teller (BET) surface area[18] and pore volume data were measured with $N_2$ at 77 K. This information was gathered for a comparison to the analysis by the MEA model. The BET surface areas are reported using a five-point BET calculation.[18] The MEA accessible surface area was calculated with $CH_4$ porosimetry. The micropore volume was determined using the Harkins−Jura *t*-plot model[19] with thickness parameters from 5.0 to 10.0 Å. Macro- and mesopore volumes were calculated using the Barrett−Joyner−Halenda (BJH) desorption curve.[20] The conclusions of the standard literature methods for characterizing the porosity of a solid are presented in Table 2.

**Adsorption Measurements.** Gas adsorption isotherms on Na−MOR and H−MOR were measured using an ASAP 2000 gas analyzer with

(14) (a) Karge, H. G.; Dondur, V. *J. Phys. Chem.* **1990**, *94*, 765−772. (b) Karge, H. G.; Dondur, V.; Weitkamp, J. *J. Phys. Chem.* **1991**, *95*, 283−288. (c) Katada, N.; Igi, H.; Kim, J.; Niwa, M. *J. Phys. Chem. B* **1997**, *101*, 5969−5977.

(15) (a) Thomas, J. M.; Klinowski, J. *Adv. Catal.* **1985**, *33*, 199−374. (b) Klinowski, J. *Chem. Rev.* **1991**, *91*, 1459−1479. (c) Pfeifer, H. *Colloids Surf.* **1989**, *36*, 169−177. (d) Xu, Q.; Eguchi, T.; Nakayam, H.; Makamura, N. *J. Chem. Soc., Faraday Trans.* **1996**, *92*, 4601−4603.

(16) (a) Wakabayashi, F. Kondo, J. N.; Wada, A.; Domen, K.; Hirose, C. *J. Phys. Chem.* **1993**, *97*, 10761−10768. (b) Wakabayashi, F.; Kondo, J. N.; Wada, A.; Domen, K.; Hirose, C. *J. Phys. Chem.* **1996**, *100*, 18882. (c) Wakabayashi, F.; Kondo, J. N.; Wada, A.; Domen, K.; Hirose, C. *Microporous Mater.* **1997**, *8*, 29−37. (d) Bordiga, S.; Lamberti, C.; Geobaldo, F.; Zecchina, A.; Palomino, G. T.; Areán, C. O. *Langmuir* **1995**, *11*, 527−533. (e) Geobaldo, F.; Lamberti, C.; Ricchiardi, G.; Bordiga, S.; Zecchina, A.; Palomino, G. T.; Areán, C. O. *J. Phys. Chem.* **1995**, *99*, 11167−11177. (f) Areán, C. O.; Palomino, G. T.; Geobaldo, F.; Zecchina, A. *J. Phys. Chem.* **1996**, *100*, 6678−6690. (g) Zecchina, A.; Geobaldo, F.; Lamberti, C.; Ricchiardi, G.; Bordiga, S. *J. Phys. Chem.* **1996**, *100*, 18883. (h) Gruver, V.; Fripiat, J. J. *J. Phys. Chem.* **1994**, *98*, 8549−8554. (i) Auroux, A.; Datka, J. *Appl. Catal. A* **1997**, *165*, 473−479. (j) Karge, H. *Z. Physik. Chem. Neue Folge* **1971**, *76*, 133−153. (k) Karge, H. G. *Z. Physik. Chem. Neue Folge* **1975**, *95*, 241−254. (l) Karge, H. G. *Z. Physik. Chem. Neue Folge* **1980**, *122*, 103−116. (m) Ward, J. W. *Zeolite Chemistry and Catalysis*; Rabo, J. A., Ed.; ACS Monograph 171; American Chemical Society: Washington, DC, 1976; pp 118−284. (n) Angell, C. L.; Scaffer, P. C. *J. Phys. Chem.* **1966**, *70*, 1413−1418.

(17) Peru, D. A.; Collins, R. J. *Fresenius J. Anal. Chem.* **1993**, *346*, 909−913.

(18) Brunauer, S.; Emmett, P. H.; Teller, E. *J. Am. Chem. Soc.* **1938**, *60*, 309−319.

(19) Harkins, W. D.; Jura, G. *J. Am. Chem. Soc.* **1944**, *66*, 1366−1373.

(20) Barrett, E. P.; Joyner, L. G.; Halenda, P. P. *J. Am. Chem. Soc.* **1951**, *73*, 373−380.

the chemisorption/physisorption software employing a 47-point pressure table from 0.1 to 760 Torr. The system was determined to have reached equilibrium when the pressure change was less than 1% of the desired pressure point in a 15-s equilibration time interval. Pressure tolerances were set to 1% for the 10-Torr transducer and 1 Torr with the 1000-Torr transducer. Low-temperature baths, consisting of liquid nitrogen/solvent mixtures,[21] were utilized to maintain a constant temperature for low-temperature experiments. For higher temperature experiments, an insulated heating mantle was used to maintain the temperature. All experiments were carried out above the critical temperature of the adsorbate—this precaution inhibits the formation of multilayers. All temperatures were maintained to within ±1 °C.

**Equilibrium Analysis.** The acquired isotherms were analyzed by using eq 3. When applying this equation, the minimum number of processes needed to attain a fit of the experimental data were utilized. Detailed criteria for selecting the correct number of processes[4c] and proper application of the multiple-process equilibrium analysis[4] have been reported. For each data set, the graph of $P_{atm}$/(number of moles adsorbed per gram) vs $P_{atm}$ produced a curved plot with linear regions. If eq 3 describes a one-process adsorption equilibrium, the transformation would produce a linear plot, with the slope equal to $1/n_1$ and the intercept equal to $1/(n_1K_1)$. The seed values for $n_i$ and $K_i$ were obtained for each process from the linear regression of the linear regions of the curved transformation plot. These seed values were employed in a program utilizing a nonlinear least-squares constrained modified simplex minimization algorithm designed to simultaneously fit the combined adsorption isotherm data of all the temperature sets for a particular adsorbate, allowing for better characterization of the processes and the total capacity of the solid. At lower temperatures, a greater proportion of the capacity of the solid is utilized, leading to a better definition of the final processes. At higher temperatures, gas uptake is significantly reduced, improving the characterization of the initial processes.

## Results and Discussion

Mordenite is a microporous zeolite with fixed channel dimensions (Figure 1). This zeolite, with reported crystallographic dimensions of 6.7 Å × 7.0 Å[9,10] for the large channel, is of interest because of its utilization in catalytic processes, such as hydrocarbon cracking.[22] The BET surface areas of Na−MOR (458 $m^2\ g^{-1}$) and H−MOR (462 $m^2\ g^{-1}$) give an inaccurate measurement of the accessible surface area because of the inherent flaws in the BET method.[1] For microporous solids, the BET model leads to a measurement that is an overestimation of the surface area.[1] Utilization of the MEA model for the analysis of gas adsorption systems with Na− and H−mordenite, above the critical temperatures of the adsorbate, yields meaningful thermodynamic parameters for the interaction of a probe with the solid and offers an alternative to the common methods of microporous solid characterization.

**Gas Adsorption on Na−Mordenite.** Na−MOR was investigated with a variety of small and large adsorbates. The smaller probe gases ($O_2$, $N_2$, CO, Ar, and $CH_4$), whose experimental and calculated isotherms at −63 °C are plotted in Figure 2, were used to better characterize the smaller channels that cannot be accessed by the larger probes. The experimental and calculated isotherms of the larger probe gases ($C_2H_6$, $C_3H_8$, $n$-$C_4H_{10}$, $i$-$C_4H_{10}$, Xe, and $SF_6$) at various temperatures are plotted in Figure 3. A variety of gases were used to better characterize the channels by gradually increasing the size of the probe in an effort to approach the channel size. The appropriate physical and molecular properties of the adsorptives can be found in Table 1. The number of processes was determined from the

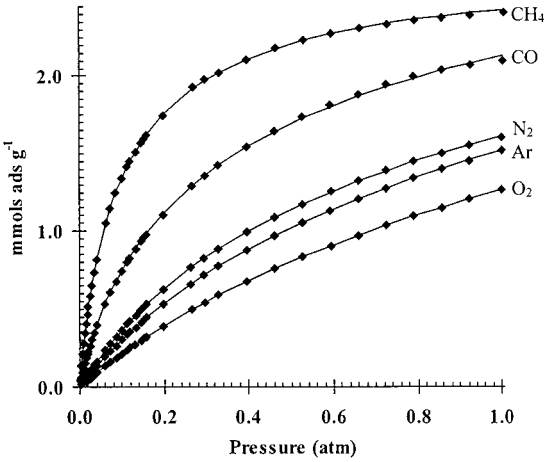


**Figure 2.** Adsorption isotherms at −63 °C for the small adsorbates ($O_2$, CO, $N_2$, Ar, and $CH_4$) on Na−mordenite. The ◆'s represent the experimental data, and the solid lines are the calculated isotherms using the $n_i$ and $K_i$ values from the MEA description of adsorption.

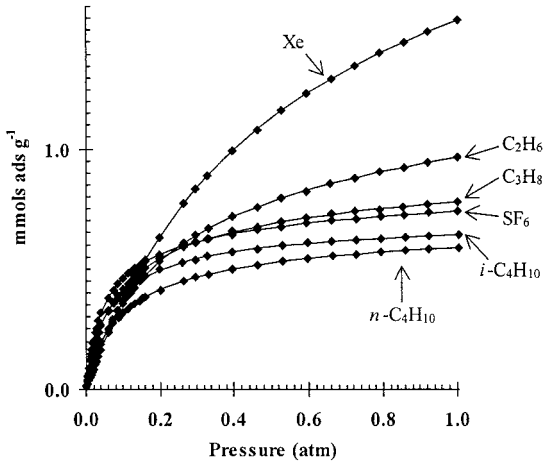


**Figure 3.** Adsorption isotherms at various temperatures for the large adsorbates Xe (30 °C), $C_2H_6$ (40 °C), $C_3H_8$ (100 °C), $SF_6$ (50 °C), $i$-$C_4H_{10}$ (140 °C), and $n$-$C_4H_{10}$ (165 °C) on Na−mordenite. The ◆'s represent the experimental data, and the solid lines are the calculated isotherms using the $n_i$ and $K_i$ values from the MEA description of adsorption.

acquired gas adsorption isotherms. The temperature-dependent $K_i$ values are listed in Table 3, and the process capacities ($n_i$), along with the accessible surface areas and pore volumes associated with each process, are reported in Table 4. The process designations emphasize the order of pore filling, with the largest $K_i$ assigned to the first process, the next largest $K_i$ assigned to the second process, and so on. Except for the weak interactions of CO and $N_2$, the work on Na−MOR lacked specific acid−base interactions, further limiting the existing number of processes. Since the smaller probes can access the small channel (while the larger probes cannot), more processes are expected for the smaller gases.

For $N_2$ and CO adsorption of Na−MOR, the extension of MEA describes three processes. $N_2$ and CO possess very specific molecular properties (i.e., size, shape, and polarizability) that enable these adsorbates to resolve two heterogeneous interactions in the large channel. CO and $N_2$ are also capable of acid−base interactions[16]—CO is weak and $N_2$ is an even weaker base. These weak donor−acceptor interactions allow for characterization of acidic properties of Na−MOR. Only two processes are required to describe $O_2$, Ar, and $CH_4$ adsorption in Na−MOR. The low polarizability (along with very little basic character)

(21) Gordon, A. J.; Ford, R. A. *The Chemist's Companion*; John Wiley and Sons: New York, 1972; p 451.

(22) (a) Bhatia, S. *Zeolite Catalysis: Principles and Applications*; CRC Press: Boca Raton, FL, 1990. (b) Iler, R. K. *The Chemistry of Silica*; John Wiley and Sons: New York, 1979.

**Table 3.** MEA Equilibrium Constants and Total Amount (mmol) Adsorbed at Lowest Temperature for Na−Mordenite

| (mmol)[a] | temp, °C | $K_1$[b] | $K_2$[b] | $K_3$[b] | (mmol)[a] | temp, °C | $K_1$[b] | $K_2$[b] | $K_3$[b] |
|---|---|---|---|---|---|---|---|---|---|
| $N_2$ | −93 | 38.69 ± 0.05 | 8.376 ± 0.019 | 0.835 ± 0.019 | CO | −93 | 267.1 ± 3.7 | 24.6 ± 1.2 | 1.6 ± 1.2 |
| (2.67) | −63 | 3.510 ± 0.031 | 1.371 ± 0.011 | 0.200 ± 0.011 | (3.17) | −63 | 14.40 ± 0.61 | 3.06 ± 0.19 | 0.29 ± 0.19 |
| | −43 | 1.490 ± 0.041 | 0.542 ± 0.014 | 0.107 ± 0.014 | | −43 | 5.422 ± 0.099 | 1.09 ± 0.03 | 0.15 ± 0.03 |
| | −19 | 0.401 ± 0.011 | 0.1902 ± 0.0039 | 0.0442 ± 0.0039 | | −19 | 1.290 ± 0.010 | 0.305 ± 0.003 | 0.062 ± 0.003 |
| Ar | −93 | 17.58 ± 0.07 | 1.87 ± 0.02 | | $O_2$ | −93 | 5.622 ± 0.097 | 0.97 ± 0.01 | |
| (2.72) | −63 | 2.55 ± 0.03 | 0.43 ± 0.01 | | (1.68) | −63 | 2.24 ± 0.01 | 0.572 ± 0.001 | |
| | −43 | 1.009 ± 0.003 | 0.2220 ± 0.0008 | | | −43 | 1.051 ± 0.014 | 0.3455 ± 0.0015 | |
| | −19 | 0.342 ± 0.006 | 0.0901 ± 0.0018 | | | | | | |
| | | | | | $C_2H_6$ | 40 | 7.420 ± 0.036 | 0.883 ± 0.035 | |
| $CH_4$ | −63 | 31.1 ± 0.2 | 6.46 ± 0.09 | | (0.96) | 55 | 4.347 ± 0.015 | 0.470 ± 0.015 | |
| (2.41) | −43 | 7.98 ± 0.17 | 2.812 ± 0.066 | | | 70 | 2.94 ± 0.01 | 0.31 ± 0.01 | |
| | −19 | 2.023 ± 0.018 | 0.7340 ± 0.0071 | | | 85 | 1.92 ± 0.01 | 0.20 ± 0.01 | |
| | | | | | | 100 | 1.317 ± 0.008 | 0.114 ± 0.008 | |
| $C_3H_8$ | 100 | 17.07 ± 0.13 | 1.78 ± 0.22 | | | | | | |
| (0.78) | 120 | 8.59 ± 0.06 | 0.776 ± 0.096 | | $n$-$C_4H_{10}$ | 165 | 18.09 ± 0.18 | 2.52 ± 0.26 | |
| | 140 | 5.14 ± 0.03 | 0.435 ± 0.053 | | (0.59) | 175 | 12.57 ± 0.07 | 1.63 ± 0.10 | |
| | 160 | 3.213 ± 0.037 | 0.249 ± 0.061 | | | 185 | 9.82 ± 0.13 | 1.253 ± 0.185 | |
| $i$-$C_4H_{10}$ | 140 | 22.55 ± 0.14 | 3.00 ± 0.39 | | Xe | 30 | 2.411 ± 0.011 | 0.976 ± 0.014 | |
| (0.64) | 155 | 16.16 ± 0.07 | 1.51 ± 0.20 | | (1.54) | 45 | 1.490 ± 0.009 | 0.530 ± 0.011 | |
| | 170 | 11.28 ± 0.05 | 1.02 ± 0.14 | | | 60 | 0.972 ± 0.003 | 0.290 ± 0.004 | |
| | 185 | 6.733 ± 0.017 | 0.408 ± 0.047 | | | 75 | 0.6689 ± 0.0036 | 0.1888 ± 0.0047 | |
| $SF_6$ | 50 | 24.56 ± 0.20 | 1.39 ± 0.45 | | | | | | |
| (0.74) | 80 | 9.316 ± 0.051 | 0.58 ± 0.11 | | | | | | |
| | 90 | 5.54 ± 0.03 | 0.306 ± 0.078 | | | | | | |

[a] Total experimental amount adsorbed (millimoles) at the lowest temperature analyzed is indicated in parentheses. [b] Gas−solid equilibrium constant. The first digit of the uncertainty is the last significant figure.

**Table 4.** MEA Process Capacities (mmol), Accessible Surface Areas ($m^2\ g^{-1}$), and Pore Volumes ($\mu L\ g^{-1}$) of Na−Mordenite[a]

| | mmol ads | area | $\mu$L ads | mmol ads | area | $\mu$L ads |
|---|---|---|---|---|---|---|
| | | $N_2$ | | | CO | |
| $n_1$ | 0.548 ± 0.011 | 50.4 ± 1.0 | 13.7 ± 0.3 | 0.530 ± 0.015 | 50.3 ± 1.4 | 15.0 ± 0.4 |
| $n_2$ | 1.587 ± 0.027 | 146.0 ± 2.4 | 39.7 ± 0.7 | 1.672 ± 0.073 | 158.8 ± 6.9 | 47.3 ± 2.1 |
| $n_3$ | 1.59 ± 0.13 | 145.9 ± 12.0 | 39.7 ± 3.3 | 1.66 ± 0.86 | 157.7 ± 81.5 | 46.9 ± 24.3 |
| total | 3.72 ± 0.17 | 342.3 ± 15.5 | 93.1 ± 4.2 | 3.86 ± 0.95 | 366.8 ± 89.9 | 109.2 ± 26.8 |
| | | Ar | | | $O_2$ | |
| $n_1$ | 0.91 ± 0.01 | 82.8 ± 0.9 | 26.3 ± 0.3 | 0.322 ± 0.005 | 28.4 ± 0.4 | 7.6 ± 0.1 |
| $n_2$ | 2.87 ± 0.05 | 262.6 ± 4.6 | 83.5 ± 1.5 | 2.85 ± 0.02 | 251.4 ± 1.9 | 67.1 ± 0.5 |
| total | 3.78 ± 0.06 | 345.3 ± 5.5 | 109.8 ± 1.7 | 3.17 ± 0.03 | 279.8 ± 2.3 | 74.7 ± 0.6 |
| | | $CH_4$ | | | $C_2H_6$ | |
| $n_1$ | 0.766 ± 0.014 | 75.0 ± 1.4 | 22.8 ± 0.4 | 0.712 ± 0.004 | 103.0 ± 0.6 | 33.6 ± 0.2 |
| $n_2$ | 1.945 ± 0.035 | 190.5 ± 3.5 | 57.9 ± 1.1 | 0.714 ± 0.035 | 103.3 ± 5.0 | 33.7 ± 1.6 |
| total | 2.71 ± 0.05 | 265.5 ± 4.9 | 80.6 ± 1.5 | 1.43 ± 0.04 | 206.2 ± 5.6 | 67.3 ± 1.8 |
| | | $C_3H_8$ | | | $n$-$C_4H_{10}$ | |
| $n_1$ | 0.5845 ± 0.0056 | 99.51 ± 0.96 | 37.72 ± 0.36 | 0.410 ± 0.005 | 87.1 ± 1.0 | 33.6 ± 0.4 |
| $n_2$ | 0.350 ± 0.056 | 59.6 ± 9.6 | 22.6 ± 3.6 | 0.278 ± 0.031 | 59.0 ± 6.7 | 22.8 ± 2.6 |
| total | 0.93 ± 0.06 | 159.1 ± 10.6 | 60.3 ± 4.0 | 0.688 ± 0.036 | 146.1 ± 7.7 | 56.4 ± 3.0 |
| | | $i$-$C_4H_{10}$ | | | $SF_6$ | |
| $n_1$ | 0.522 ± 0.004 | 120.7 ± 0.8 | 42.5 ± 0.3 | 0.6059 ± 0.0045 | 113.7 ± 0.9 | 46.7 ± 0.4 |
| $n_2$ | 0.186 ± 0.025 | 42.9 ± 5.8 | 15.1 ± 2.0 | 0.267 ± 0.072 | 50.2 ± 13.4 | 20.6 ± 5.5 |
| total | 0.708 ± 0.028 | 163.6 ± 6.6 | 57.6 ± 2.3 | 0.873 ± 0.076 | 163.9 ± 14.3 | 67.3 ± 5.9 |
| | | Xe | | | | |
| $n_1$ | 1.406 ± 0.007 | 159.4 ± 0.8 | 63.1 ± 0.4 | | | |
| $n_2$ | 1.101 ± 0.021 | 124.8 ± 2.4 | 49.3 ± 1.0 | | | |
| total | 2.51 ± 0.03 | 284.2 ± 3.3 | 112.4 ± 1.3 | | | |

[a] For excluded molecular areas and calculated molar volumes, see Table 1. The first digit of the uncertainty is the last significant figure.

and small size of $O_2$ and Ar result in their inability to distinguish two processes for adsorption in the large channel and lead to one process for the small channel and one for the large channel. It follows that, if Ar requires two processes to describe adsorption, then $O_2$ would require no more than two processes because $O_2$ has a lower polarizability than Ar. Even though $CH_4$ is more polarizable and capable of strong interactions with the solid, $CH_4$ requires two processes to describe adsorption—one process for the small channel and one for the large channel. Interestingly, while $CH_4$ demonstrates only two processes in Na−MOR, it is capable of distinguishing four processes in H−MOR (vide infra). The large adsorbates ($C_2H_6$, $C_3H_8$, $n$-$C_4H_{10}$, $i$-$C_4H_{10}$, Xe, and $SF_6$) are restricted from the small channel and are able to distinguish two heterogeneous interactions in the large channel, thereby, requiring two processes to describe adsorption.

Substitution of the calculated $n_i$ and $K_i$ into eq 3 generates the process-resolved isotherm. Figure 4 depicts a $N_2$ resolved

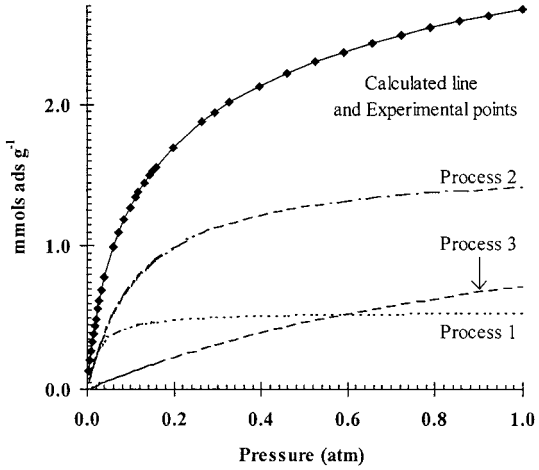


**Figure 4.** Resolved adsorption isotherm for $N_2$ on Na−mordenite at −93 °C. The ◆'s represent the experimental data, the solid line is the MEA calculated total isotherm, and the three dashed lines represent the process components.

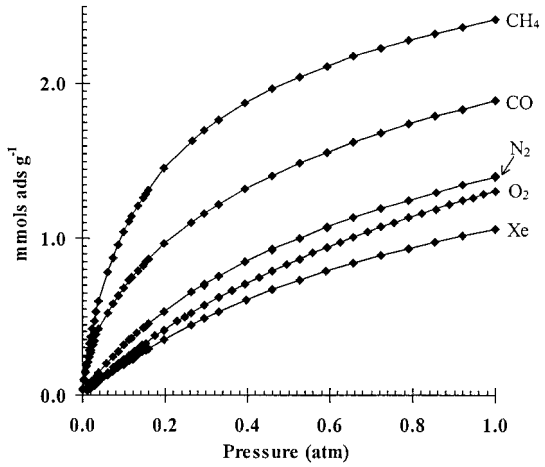


**Figure 5.** Adsorption isotherms at various temperatures for the adsorbates $O_2$ (−63 °C), $N_2$ (−63 °C), CO (−63 °C), $CH_4$ (−63 °C), and Xe (45 °C) on H−mordenite. The ◆'s represent the experimental data, and the solid lines are the calculated isotherms using the $n_i$ and $K_i$ values from the MEA description of adsorption.

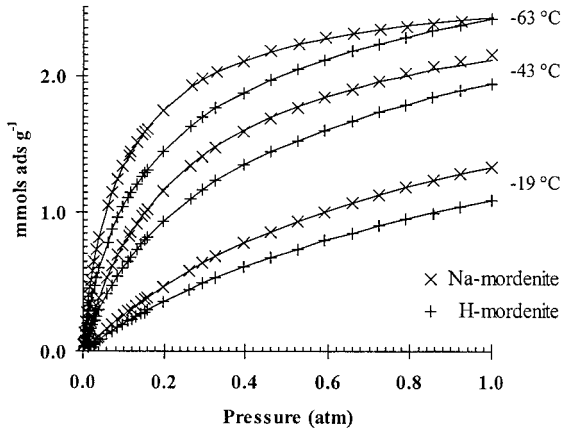


**Figure 6.** Comparison of the adsorption isotherms at various temperatures (−63, −43, and −19 °C) for $CH_4$ on H−MOR and Na−MOR. The points represent the experimental data, and the solid lines are the calculated isotherms using the $n_i$ and $K_i$ values from the MEA description of adsorption.

adsorption isotherm at −93 °C on Na−MOR. The calculated isotherm (solid line) reflects the summation of the three-component processes, demonstrating the energetically unique interactions that occur between $N_2$ and Na−MOR, and generates the experimentally determined isotherm (points) over the entire pressure range. The capability of the MEA to quantitatively predict adsorption isotherms has been discussed elsewhere—MEA can predict adsorption isotherms at higher pressures and isotherms at other temperatures (either extrapolated or interpolated).[23]

**Gas Adsorption on H−Mordenite.** The adsorption isotherms for H−MOR have been determined for $O_2$, $N_2$, CO, $CH_4$, and Xe at various temperatures. $N_2$ and $CH_4$ were chosen because they are the adsorbate standards for the BET and MEA gas adsorption models, respectively. CO was chosen because of its ability to undergo specific donor−acceptor interactions. Xe is of interest because it is slightly larger than methane and is easily polarizable. Since adsorption of the smaller and less polarizable $O_2$ on Na−MOR required only two processes (but still enters both channels), the adsorption of $O_2$ on H−MOR presents an interesting contrast to the other adsorbates. The H−MOR adsorption isotherms for Xe at 45 °C and $O_2$, $N_2$, CO, and $CH_4$ at −63 °C are plotted in Figure 5, with calculated line and experimental points. The interaction of $CH_4$ with H−MOR is interesting because of the stark differences from the results of $CH_4$ with Na−MOR—in the case of H−MOR, the description of adsorption of $CH_4$ requires two additional processes. The exchange of $Na^+$ for $H^+$ eliminates any occlusion due to the larger $Na^+$ and increases the charge-to-size ratio of the cation. Since $Na^+$ binding in zeolites is very ionic, while $H^+$ is bound with more covalent character, the $Na^+$ of Na−MOR introduces more electrostatic interactions than would be observed for H−MOR. These changes allow greater access and increased interactions in the small channel for $CH_4$. These added interactions are due to the high polarizability of $CH_4$, the size of $CH_4$, and the increased charge-to-size ratio of the cation from Na−MOR to H−MOR.

A comparison between the $CH_4$ isotherms with Na−MOR and H−MOR at several temperatures is made in Figure 6. It can be noted that Na−MOR adsorbs more of each adsorbate than does H−MOR at a given pressure below 1 atm, but the total adsorption capacity is greater for H−MOR—3.53 mmol $g^{-1}$ for H−MOR and 2.71 mmol $g^{-1}$ for Na−MOR (from the sum of the process capacities from Tables 4 and 6). The composite processes control the amount adsorbed at any given pressure—higher pressures are required to complete the total adsorption capacity of H−MOR, even though it has a greater total capacity than Na−MOR. While the same trend is observed for $O_2$—the total process capacity of H−MOR for $O_2$ (3.59 mmol $g^{-1}$) is higher than that of Na−MOR (3.17 mmol $g^{-1}$)—the total adsorption capacity of Na−MOR for $N_2$, CO, and Xe is higher than the capacity of H−MOR (Tables 4 and 6). The total adsorption capacity of a given solid for an adsorbate should not be confused with the amount adsorbed at any given pressure and temperature—raising the pressure and lowering the temperature will (generally) increase the amount adsorbed but will not change the total adsorption capacity. This concept is fundamental to the MEA interpretation.

Replacement of $Na^+$ with the much smaller $H^+$ should yield an increase in the accessible surface area of the adsorbent. The BET model finds an apparent increase in the surface area from 458 ($Na^+$ form) to 462 $m^2$ $g^{-1}$ ($H^+$ form). This small increase demonstrates the ineffectiveness of the BET model to determine an accessible surface area of a microporous solid. This inac-

(23) Webster, C. E.; Drago, R. S. *Microporous Mesoporous Mater.* **1999**, *33*, 291−306.

**Table 5.** MEA Process Capacities (mmol), Accessible Surface Areas ($m^2\ g^{-1}$), and Pore Volumes ($\mu L\ g^{-1}$) of H−Mordenite

| | temp, °C (mmol)[a] | $K_1$[b] | $K_2$[b] | $K_3$[b] | $K_4$[b] |
|---|---|---|---|---|---|
| $O_2$ | −93 (2.57) | 21.8 ± 0.3 | 2.20 ± 0.04 | | |
| | −63 | 1.043 ± 0.004 | 0.2324 ± 0.0007 | | |
| | −43 | 2.61 ± 0.04 | 0.450 ± 0.005 | | |
| | −19 | 0.305 ± 0.001 | 0.1029 ± 0.0002 | | |
| $N_2$ | −93 (2.22) | 143 ± 3 | 17.3 ± 0.4 | 1.75 ± 0.15 | |
| | −63 | 11.3 ± 0.3 | 2.476 ± 0.036 | 0.521 ± 0.014 | |
| | −43 | 3.500 ± 0.065 | 1.020 ± 0.007 | 0.228 ± 0.003 | |
| | −19 | 1.398 ± 0.021 | 0.248 ± 0.002 | 0.1068 ± 0.0009 | |
| CO | −93 (2.91) | 2078 ± 7 | 114.9 ± 3.7 | 15.0 ± 1.4 | 1.6 ± 0.9 |
| | −63 | 114.6 ± 0.4 | 9.4 ± 0.2 | 1.97 ± 0.08 | 0.35 ± 0.05 |
| | −43 | 29.71 ± 0.16 | 3.24 ± 0.08 | 0.87 ± 0.03 | 0.18 ± 0.02 |
| | −19 | 2.81 ± 0.03 | 0.249 ± 0.015 | 0.193 ± 0.006 | 0.137 ± 0.004 |
| $CH_4$ | −63 (2.41) | 54.6 ± 0.6 | 10.6 ± 0.1 | 4.5 ± 0.1 | 0.58 ± 0.09 |
| | −43 | 13.4 ± 0.1 | 4.57 ± 0.03 | 1.82 ± 0.02 | 0.29 ± 0.02 |
| | −19 | 2.83 ± 0.03 | 1.109 ± 0.006 | 0.514 ± 0.005 | 0.077 ± 0.004 |
| Xe | 30 (1.27) | 1.977 ± 0.004 | 0.370 ± 0.006 | | |
| | 45 | 1.268 ± 0.007 | 0.27 ± 0.01 | | |
| | 60 | 0.810 ± 0.004 | 0.154 ± 0.006 | | |
| | 75 | 0.551 ± 0.004 | 0.069 ± 0.007 | | |

[a] Total experimental amount adsorbed (mmol) at the lowest temperature analyzed is indicated in parentheses. [b] Gas−solid equilibrium constant. The first digit of the uncertainty is the last significant figure.

**Table 6.** MEA Accessible Surface Areas ($m^2\ g^{-1}$) and Volumes ($\mu L\ g^{-1}$) of H−Mordenite[a]

| | mmol ads | area | $\mu$L ads | mmol ads | area | $\mu$L ads | mmol ads | area | $\mu$L ads |
|---|---|---|---|---|---|---|---|---|---|
| | $O_2$ | | | $N_2$ | | | Xe | | |
| $n_1$ | 0.470 ± 0.008 | 41.5 ± 0.7 | 11.1 ± 0.2 | 0.094 ± 0.003 | 8.67 ± 0.25 | 2.359 ± 0.069 | 1.547 ± 0.009 | 175.4 ± 1.0 | 69.4 ± 0.4 |
| $n_2$ | 3.12 ± 0.04 | 275.2 ± 3.4 | 73.4 ± 0.9 | 0.82 ± 0.01 | 75.9 ± 1.2 | 20.6 ± 0.3 | 0.92 ± 0.05 | 103.9 ± 6.0 | 41.1 ± 2.4 |
| $n_3$ | | | | 2.12 ± 0.11 | 195.1 ± 9.8 | 53.1 ± 2.7 | | | |
| total | 3.59 ± 0.05 | 316.7 ± 4.1 | 84.5 ± 1.1 | 3.04 ± 0.12 | 279.6 ± 11.3 | 76.1 ± 3.1 | 2.46 ± 0.06 | 279.3 ± 7.0 | 110.5 ± 2.8 |
| | CO | | | $CH_4$ | | | | | |
| $n_1$ | 0.231 ± 0.002 | 22.0 ± 0.2 | 6.54 ± 0.05 | 0.191 ± 0.002 | 18.7 ± 0.2 | 5.67 ± 0.07 | | | |
| $n_2$ | 0.45 ± 0.02 | 42.5 ± 1.6 | 12.6 ± 0.5 | 0.932 ± 0.008 | 91.3 ± 0.8 | 27.7 ± 0.2 | | | |
| $n_3$ | 1.20 ± 0.07 | 114.1 ± 6.7 | 34.0 ± 2.0 | 1.07 ± 0.02 | 105.2 ± 1.8 | 31.9 ± 0.6 | | | |
| $n_4$ | 1.8 ± 0.6 | 170 ± 56 | 51 ± 17 | 1.34 ± 0.14 | 130.9 ± 13.6 | 39.7 ± 4.1 | | | |
| total | 3.7 ± 0.7 | 349 ± 64 | 104 ± 19 | 3.53 ± 0.17 | 346 ± 16 | 105 ± 5 | | | |

[a] For excluded molecular areas and calculated molar volumes, see Table 1. The first digit of the uncertainty is the last significant figure.

curacy exists because the experiment of the BET model fills a microporous structure with liquid nitrogen and designates the result as a surface area measurement. Therefore, the slight differences in the BET surface areas can be attributed to the difference in volume between $Na^+$ and $H^+$ cations. In contrast, MEA determined the accessible surface area of Na−MOR to be 265 $m^2\ g^{-1}$ and that of H−MOR to be 346 $m^2\ g^{-1}$. These values are significantly different because of the increased interactions of $CH_4$ in both channels of H−MOR. The temperature-dependent thermodynamic equilibrium constants ($K_i$) for the adsorbates with H−MOR are listed in Table 5; process capacities ($n_i$), accessible process surface areas, and pore volumes for the adsorbates with H−MOR are tabulated in Table 6.

**Summary of Na−Mordenite and H−Mordenite Thermodynamic Data.** A solid with a limited pore size distribution undergoes different types of adsorbate−adsorbent interactions than does an amorphous solid. The distinction between interactions is clarified through the use of the process and type terminology.[4d] A type 1 interaction arises when the probe undergoes strong interactions with all sides of the pore, i.e., when the probe size most closely matches the pore size. A type 2 interaction is an interaction with one wall and a significant, yet smaller, interaction with the opposite wall. A type 3 interaction is adsorption on a surface with no significant interaction from the opposing wall. The difference between process and type designation is that processes describe the order of pore filling, while types classify the interactions of a probe with the adsorbent. (In an effort to avoid confusion, $\Delta H_i$ and $\Delta S_i$ have been used to represent process-designated enthalpies and entropies, while $\Delta H_t$ and $\Delta S_t$ represent type-designated enthalpies and entropies.) A process is determined simply by ordering the $K_i$ from largest to smallest, with the largest $K_i$ corresponding to the first process, etc. In general, the order of the enthalpies of adsorption follows the order of the process designations—no reversal of ordering of $K_i$ and $\Delta H_i$. If there is a reversal, in general, to determine the type designation for a given process, one orders the entropies of adsorption for the processes and assigns the least negative entropy to the type 3, the next least negative entropy to type 2, and so on. This type designation may be complicated by a probe that does not undergo a particular type interaction with the adsorbent, e.g., no type 1 interaction or interactions of a particular probe with the heterogeneity of the solid (vide infra). The $\Delta H_t$ vs $a^{1/2}$ (square root of the van der Waals $a$ parameter) plots are also useful in distinguishing type designations in a given adsorbate−adsorbent system.

Previous studies have explored porous carbons where process and type designations are indistinguishable.[4a−c,24] The similarity of process and type designations is a result of the wide pore size distribution that allows the probe gas to "choose" the mostthermodynamically favored pore. In amorphous solids, gas adsorption occurs in pores similar in size to the probe gas, necessarily leading to the largest $K_i$ and the most negative $\Delta H_i$

(24) Kassel, W. S. Ph.D. Thesis, University of Florida, 1998.

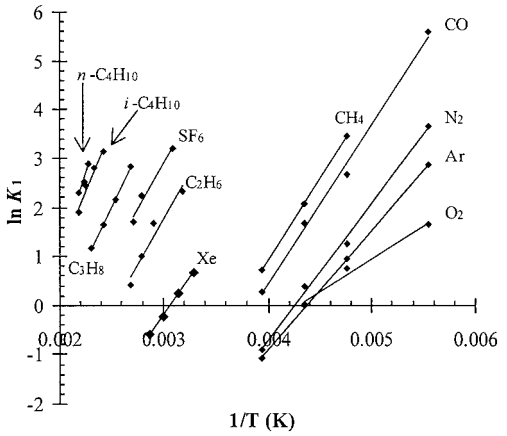


**Figure 7.** Example of van't Hoff plots (ln $K_i$ vs $1/T$ (K)) for the various adsorbates on Na−mordenite.

corresponding to the same process.[4a−c] A study of the zeolite HZSM-5[4d] found that there is no direct correlation between types and processes because, in contrast to amorphous carbons, zeolites have fixed pore sizes. The probe adsorbs in the limited pore structure of the zeolite, which is not necessarily the "ideal" size for the adsorbate—e.g., mordenite offers two unique channels for gas adsorption. Since crystalline solids have a limited pore structure that dictates where and how gas adsorption will occur, types and processes need not correlate.

Recall that type 1 is defined as a strong interaction with two opposing walls. The small gases ($O_2$, $N_2$, CO, Ar, and $CH_4$) are of an appropriate size to enter the small channel of mordenite, where the strongest interactions for the smaller probes can occur. For the small probes in the resolved isotherm, the first process corresponds to some variant of type 1 or type 2 adsorption in the small channel. The resolved isotherm illustrates two processes for $N_2$ and CO occurring in the large channel of mordenite, corresponding to two unique adsorbate−adsorbent interactions in the large channel. As discussed earlier, $O_2$ and Ar cannot distinguish heterogeneous interactions in the large channel. Most of the larger probes ($C_3H_8$, *n*-$C_4H_{10}$, *i*-$C_4H_{10}$, Xe, and $SF_6$) cannot fit adjacent to each other in the large channel of mordenite. The larger probes studied cannot access the small channel and are too small to undergo more than moderate interactions with the opposing wall of the large channel. For these molecules, the absence of strong interactions with two opposing walls leads to no type 1 interactions. However, by default, there is a first process because there is a largest $K_i$. In general, as the size of a given adsorbate increases, the excluded molecular area and the interactions with the channel increase, leading to a more negative $\Delta H_i$. The resolved isotherms for the large probes illustrate two different processes. Since the dimensions of the larger molecules are larger than the free aperture of the small channel, these two distinct processes must occur in the main channel.

The enthalpies and entropies of adsorption for each process and adsorbate are determined from a van't Hoff plot with a weighted linear regression (e.g., Figure 7 for the first process of the adsorbates interacting with Na−MOR). The thermodynamic parameters for each adsorbate and process can be found in Table 7 (Na−MOR) and Table 8 (H−MOR). For each of the adsorptives, the experiments are performed above the critical temperature of the gas. One should remember that the enthalpy of vaporization of a liquid becomes zero (as does the entropy of vaporization) as the temperature of the liquid approaches its critical temperature.

**Entropy of Adsorption.** One might expect that the difference between the process entropies for the small adsorptives would result from simply confining the adsorbate to the smaller of the two channels (resulting from a change in volume). This difference in volume would produce a difference of 2.9 eu (2.9 eu $= -R \ln(v_{small}/v_{large}) = R \ln(26.3/112.4)$; 26.3 $\mu$L from the first Ar process with Na−MOR, and 112.4 $\mu$L from the total of the Xe processes with Na−MOR). However, the largest observed difference is 13.9 eu. Therefore, the difference in the process entropies results from the differing interactions of the adsorbate with the solid.

One might note that, in general, the entropy of adsorption is relatively constant, $\sim -22$ eu. One can compare the magnitude of this average of the entropies of adsorption (22 eu) to Trouton's constant (21−22 eu). With Trouton's rule, the relationship comes from the similarity of the dispersion interaction of the molecules at the phase transition. The phase transition produces a change in the environment of a molecule from the gas phase, where it has free motion, to the liquid phase, where it has restricted motion. One would expect that a physisorption interaction would also produce a similar restrictive motion due to the dispersion interaction, more specifically, the interaction of the molecule with a homogeneous portion of the solid. This constancy of the entropy of adsorption is analogous to Trouton's rule; i.e., for a given molecule interacting with a solid, the entropy of adsorption remains approximately constant, as for a pseudo-phase change of the adsorptive. The variation of the entropy from 22 eu is due to the influence of the solid on the adsorbate. The deviation of $O_2$ from this entropy relationship when interacting with Na−MOR ($\Delta S_i = 11.4 \pm 2.3$ and $9.6 \pm 1.9$) could be due to its low polarizability. $O_2$ interacting with Na−MOR also has a smaller than expected magnitude in its enthalpy of adsorption when compared to other adsorbates ($\Delta H_i = 2.71 \pm 0.47$ and $1.75 \pm 0.41$) (vide infra, Figure 9).

**Process and Type Designations.** For the smaller adsorbates ($O_2$, $N_2$, CO, Ar, and $CH_4$), the process designations are in the same order as the type designations (Tables 7 and 8). With most of the larger probes ($C_2H_6$, $C_3H_8$, *n*-$C_4H_{10}$, *i*-$C_4H_{10}$, and Xe), more negative $\Delta H_2$ and $\Delta S_2$ (the second process) are found when compared to those determined for the first process for Na−MOR (Table 7). For the large adsorbates, the reversal of the order of the enthalpy and entropy of adsorption for the first and second process occurs because of the different interaction types between the adsorbate and adsorbent. This reversal is also found for Xe on H−MOR (Table 8).

**Linear Correlations of Thermodynamic Parameters.** An increase in magnitude of the entropy is generally observed[25] with a more negative enthalpy of interaction. This relationship has also been reported for solubility data and was first compiled by Barclay and Butler.[25b] Figure 8a−c represents the linearity of the entropy−enthalpy plots ($-\Delta S_t$ versus $-\Delta H_t$) for CO, $C_2H_6$, and $SF_6$ on a variety of solids, which illustrates process and type designations. Error bars are included for the parameters derived for the carbonaceous solids; where no error bars are visible, they are present underneath the symbol for that particular data point. For the carbonaceous solids (A572, A600, A563, F300, and BPL),[24] the process and type designations concur on CO, $C_2H_6$, and $SF_6$. Recall that process designations are simply the order of pore filling (highest $K_i$ first). For the zeolitic solids (HZSM-5 and Na−MOR)—where process and type designations need not correspond—the first process for $C_2H_6$ and $SF_6$ on Na−MOR is a type 2 interaction, the $C_2H_6$ and $SF_6$ second

(25) (a) Person, W. B. *J. Am. Chem. Soc.* **1962**, *84*, 536−540. (b) Barclay, I. M.; Butler, J. A. V. *Trans. Faraday Soc.* **1938**, *34*, 1445−1454.

**Table 7.** Process-Designated Enthalpies and Entropies of Adsorption with Na−Mordenite[a]

| | $-\Delta H_1$ | $-\Delta S_1$ | $-\Delta H_2$ | $-\Delta S_2$ | $-\Delta H_3$ | $-\Delta S_3$ |
|---|---|---|---|---|---|---|
| $N_2$ | 5.67 ± 0.38 | 24.3 ± 2.0 | 4.59 ± 0.11 | 21.3 ± 0.6 | 3.56 ± 0.18 | 20.1 ± 0.9 |
| CO | 6.46 ± 0.33 | 24.8 ± 1.5 | 5.37 ± 0.11 | 23.4 ± 0.5 | 3.93 ± 0.12 | 20.9 ± 0.5 |
| Ar | 4.7 ± 0.1 | 20.7 ± 0.5 | 3.60 ± 0.17 | 18.7 ± 0.8 | | |
| $O_2$ | 2.71 ± 0.47 | 11.4 ± 2.3 | 1.75 ± 0.41 | 9.6 ± 1.9 | | |
| $CH_4$ | 6.46 ± 0.52 | 24.0 ± 2.3 | 5.18 ± 0.23 | 20.9 ± 1.0 | | |
| $C_2H_6$ | 6.60 ± 0.12 | 17.14 ± 0.36 | 7.53 ± 0.40 | 24.3 ± 1.2 | | |
| $C_3H_8$ | 8.92 ± 0.34 | 18.34 ± 0.84 | 10.52 ± 0.48 | 27.1 ± 1.2 | | |
| *n*-$C_4H_{10}$ | 12.4 ± 1.5 | 22.5 ± 3.3 | 14.2 ± 2.3 | 30.7 ± 5.0 | | |
| *i*-$C_4H_{10}$ | 10.4 ± 1.0 | 18.7 ± 2.3 | 16.1 ± 1.9 | 36.7 ± 4.5 | | |
| Xe | 5.995 ± 0.067 | 18.04 ± 0.21 | 7.82 ± 0.26 | 25.85 ± 0.81 | | |
| $SF_6$ | 7.4 ± 1.3 | 16.5 ± 3.7 | 7.3 ± 2.0 | 21.8 ± 5.7 | | |

[a] The process-designated enthalpies and entropies head the table columns. Enthalpies in kcal mol$^{-1}$ and entropies in eu (cal mol$^{-1}$ K$^{-1}$). The first digit of the uncertainty is the last significant figure.

**Table 8.** Process-Designated Enthalpies and Entropies of Adsorption with H−Mordenite[a]

| | $-\Delta H_1$ | $-\Delta S_1$ | $-\Delta H_2$ | $-\Delta S_2$ | $-\Delta H_3$ | $-\Delta S_3$ | $-\Delta H_4$ | $-\Delta S_4$ |
|---|---|---|---|---|---|---|---|---|
| $O_2$ | 5.2 ± 0.2 | 22.8 ± 0.8 | 3.7 ± 0.1 | 19.2 ± 0.5 | | | | |
| $N_2$ | 5.70 ± 0.31 | 22.0 ± 1.4 | 5.17 ± 0.33 | 22.8 ± 1.5 | 3.59 ± 0.19 | 18.6 ± 0.8 | | |
| CO | 7.6 ± 0.7 | 26.8 ± 3.5 | 6.8 ± 1.1 | 28.0 ± 5.2 | 5.3 ± 0.4 | 24.0 ± 1.8 | 2.6 ± 0.6 | 14.1 ± 2.6 |
| $CH_4$ | 7.1 ± 0.2 | 25.99 ± 0.97 | 5.7 ± 0.9 | 22.0 ± 3.7 | 5.4 ± 0.5 | 22.5 ± 2.3 | 5.3 ± 1.0 | 25.6 ± 4.4 |
| Xe | 5.96 ± 0.09 | 18.3 ± 0.3 | 6.8 ± 1.5 | 24.2 ± 4.8 | | | | |

[a] The process-designated enthalpies and entropies head the table columns. Enthalpies in kcal mol$^{-1}$ and entropies in eu (cal mol$^{-1}$ K$^{-1}$). The first digit of the uncertainty is the last significant figure.

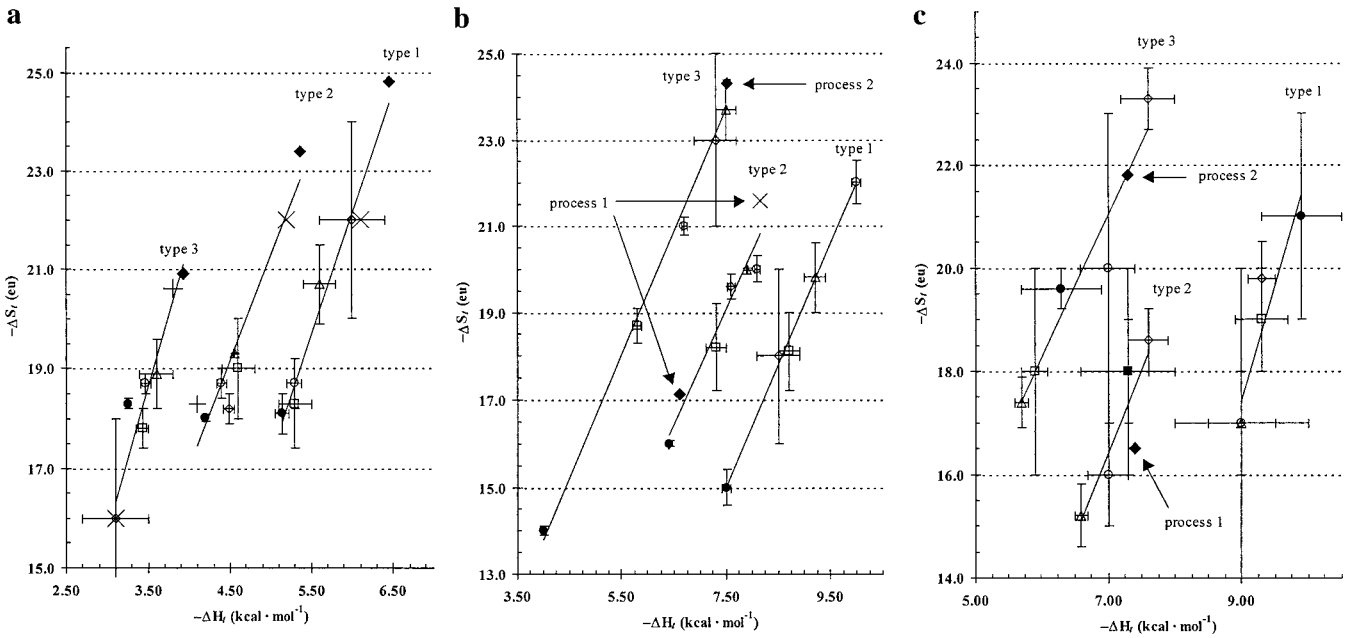


**Figure 8.** When the adsorption processes are grouped according to the interaction type, the graph of the entropy vs the enthalpy of adsorption ($-\Delta S_t$ vs $-\Delta H_t$) results in a linear correlation. (a) CO type plot, (b) $C_2H_6$ type plot, and (c) $SF_6$ type plot. The symbols are as follow: ●, BPL; ○, A572; △, A600; □, F300; ◇, A563; ◆, Na−MOR; ×, HZSM-5; and +, TS-1.

process on Na−MOR is a type 3, and the first $C_2H_6$ process on HZSM-5 is a type 2 interaction. The type designations for $C_2H_6$ and $SF_6$ are not what are expected from the $-\Delta H_t$ vs $a^{1/2}$ plot (see Figure 9). For all of the CO systems (except TS-1 with no type 1 interaction), the process and type designations coincide. One should note that the separation of the types is derived from the enthalpy data, which have significantly lower errors than the entropy data. While the CO, $C_2H_6$, and $SF_6$ plots best represent the difference in type and process designations, equivalent plots can be made for other adsorbates and show similar trends.

Entropy−enthalpy type plots could be representative of the pore size distribution (PSD) of the solids involved in the gas−solid interactions. One could envision the closer the size of the pore and the adsorbate molecule, the "tighter" the fit of the molecule in the pore. For a given type of interaction (i.e., a small range of enthalpies), the entropy of adsorption is governed by the "tightness" of the fit which the molecule involved in the interaction experiences (i.e., the PSD of the solid). Therefore, the entropy and enthalpy coordinates on a type plot are governed by two factors—the adsorbate and the PSD of the adsorbent. For adsorbents that have pores that do not fit the "ideal distribution" preferred by the adsorbate, the points for those adsorbates could deviate from the entropy−enthalpy plots of the carbonaceous solids, which have a very wide pore size distribution.

For example, considering the interaction of $C_2H_6$ with the solids Na−MOR and HZSM-5 (which have a known, limited, and fixed PSD), the interpretation of the PSD from the $C_2H_6$ type plot is corroborated. The type 3 interaction for $C_2H_6$ with

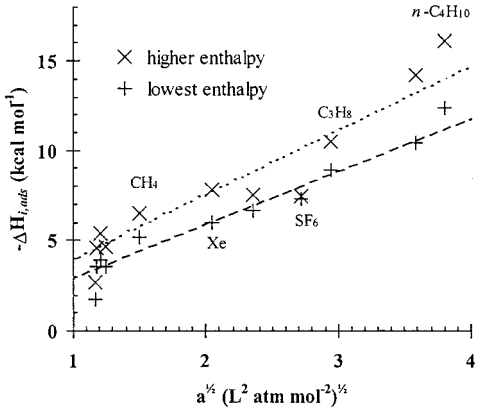


**Figure 9.** Type-grouped enthalpies of adsorption ($-\Delta H_{t,ads}$) for the adsorbates on Na−mordenite versus the square root of the van der Waals *a* parameters ($a^{1/2}$) of the adsorbates with the weighted linear regression line.

Na−MOR has a large magnitude $\Delta S$, indicative of the very limited pore size distribution of Na−MOR. Compared to the pores of the carbonaceous solids, which have a more extensive PSD, the large channel of mordenite has static dimensions of 6.7 Å × 7.0 Å; i.e., the carbonaceous solids have a large number of pores with sizes larger than two ethane molecular diameters. For Na−MOR, the other resolved interaction of $C_2H_6$ fits on the type 2 correlation with a low magnitude $\Delta S$ because of the pore size of the large channel of mordenite compared to the size of $C_2H_6$. The pore size distribution of HZSM-5 available to $C_2H_6$ for adsorption is very limited and is on the order of 1.2 but less than 1.5 molecular diameters. $C_2H_6$ interacting with HZSM-5 fits well on the type 2 correlation with a high magnitude $\Delta S$.

It is also interesting to note that, for the adsorbates interacting with both Na− and H−MOR, the enthalpy of adsorption ($\Delta H_i$) is directly proportional to the temperature-dependent change in free energy ($\Delta G_i$). Of course, this linear relationship can be observed only for adsorbates that require more than two processes. The highest enthalpy process for $N_2$ and CO interacting with H−MOR and the lowest process enthalpy for $CH_4$ interacting with H−MOR deviate from this relationship, and this departure is an indication of a nonsimilar adsorption process, when compared to the other processes. The deviation of the strongest interaction of $N_2$ and CO might be expected since these processes are most likely the interaction with the most acidic acid site of H−MOR.

Larger $K_i$ (Table 5) and higher magnitude $\Delta H_i$ (Table 8) are observed for the interactions of the adsorbate with H−MOR when compared to those with Na−MOR. These changes indicate that, while the $H^+$ in H−MOR is not able to significantly hinder adsorption (as did the $Na^+$), the proton influences the adsorbate−adsorbent interactions considerably. The values of $\Delta H_1$ and $\Delta H_3$ for $N_2$ remain constant (within error) for the interaction with H−MOR and Na−MOR (Tables 7 and 8). Geobaldo et al. conclude that the strongest interaction of $N_2$ with H−MOR is with the Lewis acid site.[16e] The $\Delta H_1$ for $N_2$ represents an interaction with the Lewis acid site, and the exchange of the $Na^+$ for the $H^+$ does not significantly affect the strength of the Lewis site. Geobaldo et al. also conclude that, while $N_2$ can access the small channel, $N_2$ does not interact with the small channel Brönsted acid site.[16e] These conclusions[16e] confirm our findings with MEA—no fourth process for the interaction of $N_2$ with H−MOR (vide infra). For $N_2$ interacting with Na−MOR and H−MOR, the low heat and constant value of $\Delta H_3$ indicate that the third process (type 3) is a simple physisorption interaction with the solid. The conclusions of Geobaldo et al. concur with this simple physisorption assignment.[16e]

In general for a given type of interaction, $\Delta H_t$ is proportional to the square root of the van der Waals *a* constant.[4] Figure 9 demonstrates the correlation that exists between the enthalpy of adsorption and $a^{1/2}$. The following adsorbates followed by process number and enthalpy are plotted in Figure 9: $O_2$ (process 1, 2.71 kcal $mol^{-1}$; process 2, 1.75 kcal $mol^{-1}$), $N_2$ (2, 4.59; 3, 3.56), CO (2, 5.37; 3, 3.93), Ar (1, 4.7; 2, 3.60), $CH_4$ (1, 6.46; 2, 5.18), Xe (1, 5.995; 2, 7.82), $C_2H_6$ (1, 6.60; 2, 7.53), $SF_6$ (1, 7.4; 2, 7.3), $C_3H_8$ (1, 8.92; 2, 10.52), *i*-$C_4H_{10}$ (1, 10.4; 2, 16.1) to *n*-$C_4H_{10}$ (1, 12.4; 2, 14.2). In general, the lowest magnitude enthalpy corresponds to a progressively higher type interaction. It should be noted that the type designations of $C_2H_6$ and $SF_6$ cannot be distinguished with the enthalpy vs $a^{1/2}$ plot—these designations have been made with the entropy−enthalpy plot (see Figure 8). In the case of $C_2H_6$, the higher magnitude enthalpy (and entropy) corresponds to a type 3 interaction; for $SF_6$, the enthalpies are the same within error and the higher magnitude entropy (the second process) also corresponds to a type 3 interaction. One possible explanation is that one of the dimensions of these molecules allows for them to interact with the eight-member oxygen ring of the side pocket of the mordenite framework with an aperture of 4.82 Å × 3.97 Å. The third minimum dimension of $C_2H_6$ (MIN-3) is 4.82 Å, and the first minimum dimension of $SF_6$ (MIN-1) is 4.87 Å.[12] The other adsorbates in this study have dimensions that are either smaller than or larger than this ~4.8 Å window. The lack of correlation between the process-designated enthalpies and $a^{1/2}$ is due to the fact that processes are not a measure of adsorbate−adsorbent interactions. The first process for the small adsorbates does not involve the same interactions as the first process for the larger adsorbates; e.g., $N_2$ (smaller adsorbate) is capable of entering the small channel, while the larger *i*-$C_4H_{10}$ is restricted from those pores. The type designation groups similar interactions and allows for the correlation with the $a^{1/2}$. For the type 3 enthalpies, the weighted linear regression of enthalpies for the adsorbates interacting with Na−MOR vs $a^{1/2}$ is $-\Delta H_3 = (3.02 \pm 0.20)a^{1/2} + (0.54 \pm 0.41)$, $R^2 = 0.96$. Poorer correlations can arise because of a finite pore size of a given adsorbent; e.g., in mordenite each probe adsorbs with the strongest possible interaction, which is not necessarily the most "ideal" interaction type, changing the expected magnitude of the enthalpy.

Each probe will maximize its interaction with one wall, and as the probe size increases, the adsorbate will begin to interact with the opposing wall. For example, a steady increase of the $-\Delta H_{t,ads}$ for type 2 on Na−MOR is observed from $CH_4$ (6.46 kcal $mol^{-1}$), $C_2H_6$ (6.60), $C_3H_8$ (10.52), *n*-$C_4H_{10}$ (14.2), to *i*-$C_4H_{10}$ (16.1). This trend demonstrates the gradual increase of adsorbate−adsorbent interactions as a probe increases the interactions with the opposite wall of the large channel. The following adsorptives, with the process listed in parentheses, are assigned to the type 2 enthalpy when interacting with Na−MOR: $O_2$ (1), $N_2$ (2), Ar (1), CO (2), $CH_4$ (1), $C_2H_6$ (1), $SF_6$ (1), Xe (2), $C_3H_8$ (2), *n*-$C_4H_{10}$ (2), and *i*-$C_4H_{10}$ (2). The weighted linear regression of the type 2 enthalpies for the adsorbates interacting with Na−MOR vs $a^{1/2}$ yields a poor correlation, $-\Delta H_2 = (3.22 \pm 0.51)a^{1/2} + (0.66 \pm 1.01)$, $R^2 = 0.82$. As one might expect, there also exists a correlation between the excluded molecular area and the enthalpy of adsorption for a given type of interaction; as the excluded molecular area increases, so does the enthalpy of adsorption.

**Comparison of MEA Results with IR Studies, Simulations, and Adsorption Studies.** Since the acidic form of mordenite (H−MOR) is often utilized in catalytic industrial processes, the complete characterization of its acidic properties is useful. Many techniques, such as temperature-programmed desorption,[14] various nuclear magnetic resonance methods,[15] and infrared spectrocopy,[16] have been employed to study the interactions between a probe molecule and mordenite. Since the MEA model has the ability to characterize heterogeneous gas−solid interactions, it is interesting to explore the differences in gas adsorption between Na−MOR and H−MOR. In addition, it is useful to compare the MEA interpretation to the pertinent results from the above-mentioned spectroscopic techniques.

Geobaldo et al. and Wakabayashi et al. have studied H−MOR and the Group IA cation exchanged forms of mordenite and found results that depend on the cation.[16a−g] The exchange of the $H^+$ with an alkali metal cation will lead to two differences in the gas−solid interactions. First, the $H^+$ will occupy considerably less space than the akali cation, thereby significantly reducing the occlusion of the small channel produced by the Group IA cations. Excluding specific interactions, this feature will lead to increased accessible surface areas. Second, the proton, with its larger charge-to-size ratio, will increase the strength of the specific interactions of the adsorbate with the solid, i.e., increased equilibrium constants ($K_i$) and enthalpies of adsorption ($\Delta H_i$). The effect of the electrostatic field of the exchanged cation on the observed $\nu_{OH}$ as well as the frequency of the adsorbed species has been well documented.[16m,n]

Since both the fundamental infrared stretching frequency of the adsorbed molecule and the change in free energy upon adsorption are proportional to the strength of the interaction (between the adsorbate and the adsorbent), one might expect a linear relationship between the free energy change associated with adsorption and the infrared stretching frequency of the adsorbed molecule. A comparison of the findings of Geobaldo et al. and Wakabayashi et al. (fundamental infrared stretching frequencies associated with the adsorbed molecule) with the MEA results (change in free energy upon adsorption) yields reasonable agreement. If one compares the $N_2$ stretching frequencies ($\nu_{N\equiv N}$) of the adsorbed $N_2$ on H−MOR[16a,e] to the natural log of the MEA-derived process equilibrium constant ($\ln K_i$, which is directly proportional to $\Delta G_i$) for $N_2$ adsorbed on H−MOR, one finds a linear correlation (see Figure 10a). The temperature-dependent thermodynamic equilibrium constants are plotted vs the observed frequency of the adsorbed $N_2$, which is not temperature dependent. This linear correlation is the expected linear free energy relationship for the simple adduct formation of a given molecule and a series of acids.[27]

Again, a linear correlation is found if one compares the analogous CO data of Bordiga et al.[16d] ($\nu_{C\equiv O}$ for the interaction of CO with H−MOR) to the MEA results ($\ln K_i$) (see Figure 10b). The IR spectrum of CO adsorbed on H−MOR contains three bands (one band at ∼2223 $cm^{-1}$, one asymmetric band at 2172 $cm^{-1}$, and one band at 2138 $cm^{-1}$).[16d] Although Bordiga et al. do not assign the broad peak centered at ∼2223 $cm^{-1}$, the peak assignment follows from the conclusions of Geobaldo et al.[16e] and the conclusions of Gruver and Fripiat[16h]—this peak is the interaction of CO with the Lewis acid site. Bordiga et al. note that the 2172-$cm^{-1}$ band is asymmetric on the low-frequency side and attribute this band to the two types of bridged

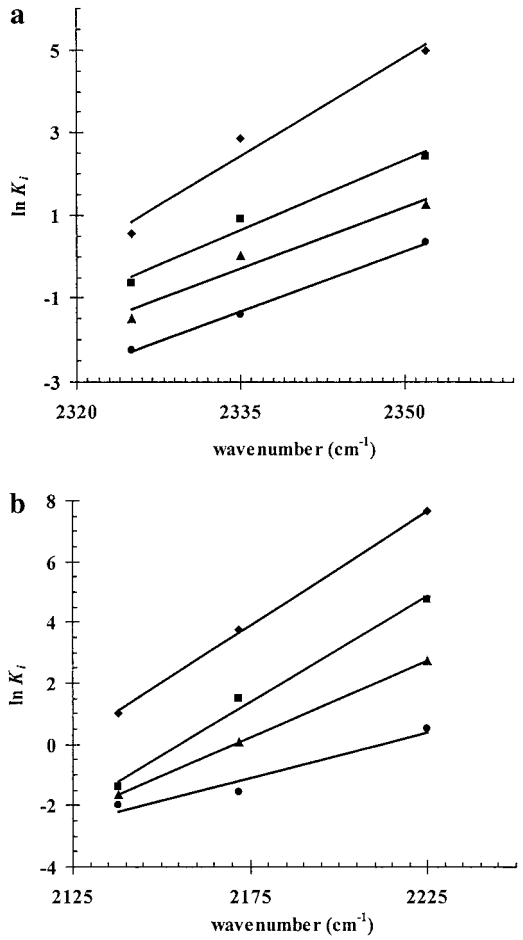


**Figure 10.** Linear free energy relationship between the temperature-dependent free energy ($\ln K_i$) and the infrared stretching frequency ($\nu$) for (a) $N_2$ adsorbed on H−mordenite at −93 (◆), −63 (■), −43 (▲), and −19 °C (●), and (b) CO adsorbed on H−mordenite at −93 (◆), −63 (■), −43 (▲), and −19 °C (●).

(Brönsted) OH groups (main channel and small channel location).[16d] While "the perturbation of the C−O stretching vibration does not seem to be sensitive enough to discriminate between the two [Brönsted sites]",[16d] MEA can resolve this slight difference in interaction. Since the 2172-$cm^{-1}$ asymmetric peak is comprised of the two unresolved interactions, Figure 10b includes the shift of this asymmetric peak once—speculation about the deconvolution of this 2172-$cm^{-1}$ band is erroneous. To match the 2172-$cm^{-1}$ shift, the value for the $\ln K_i$ used in Figure 10b is the capacity-weighted free energy change for the second and third process, $\ln K_{2-3\ \text{weighted}} = (n_2/(n_2 + n_3)) \ln K_2 + (n_3/(n_2 + n_3)) \ln K_3$. From the process capacities, one can conclude that the second CO process on H−MOR is associated with the interaction with the Brönsted sites in the small channel, while the third CO process is associated with the interaction with the large channel Brönsted acid site.

The restrictive size and geometry of the mordenite large channel requires the probe molecules to encounter different gas−solid interactions in the same channel. In the large channel, adsorption at adjacent walls is eliminated for the large probes, and the structure of the large channel forces adsorbate−adsorbent interactions that are energetically unique. The MEA description of adsorption distinguishes between two unique interactions in the large channel for Xe (5.995 ± 0.067 kcal $mol^{-1}$ for the first process [type 3] and 7.82 ± 0.26 kcal $mol^{-1}$ for the second process [type 2]), and this finding is in agreement with the Monte Carlo simulations of Xe adsorption on Na−

(26) Nivarthi, S. S.; Van Tassel, P. R.; Davis, H. T.; McCormick, A. V. *J. Chem. Phys.* **1995**, *103*, 3029−3037.

(27) Joesten, M. D.; Drago, R. S. *J. Am. Chem. Soc*. **1962**, *84*, 3817−3821.

MOR.[26] From Monte Carlo simulations, Nivathi et al. conclude that there are two heterogeneous adsorption processes—one process at the opening to the side pockets in the main channel (two "sites") with an enthalpy of 10.7 kcal mol$^{-1}$ and the other process in the main channel (six "sites") with an enthalpy of 7.2 kcal mol$^{-1}$.[26] The authors state that two of the six "sites" of the main channel have a slightly different adsorption potential, a difference of 0.09 kcal mol$^{-1}$ for a Si/Al ratio of 5, which is within two standard deviations of the MEA enthalpy for the first process (type 3). Since there exists an "inaccurate estimation of the polarization energy component of the total adsorption potential energy",[26] the ratio of the enthalpies from the simulation ($\Delta H_{\text{side pocket}}/\Delta H_{\text{main}} = 0.67$) and the ratio of the MEA enthalpies ($\Delta H_{\text{process 1}}/\Delta H_{\text{process 2}} = 0.77$) should be used for a comparison. This comparison of the relative values demonstrates modest agreement between the two. For a comparison of the amount of Xe adsorbed by Na−MOR for a given process, a ratio of the process capacity to the total capacity should be used. This comparison yields $0.37 \pm 0.1$[28] for the second MEA process capacity and 0.25[29] for the "side-pocket site" capacity.

Ohgushi and Yokoyama have reported the heat of adsorption for Xe in Na−MOR (Si/Al = 9.43) to be ~7.6 kcal mol$^{-1}$,[30] and this value is in good agreement with the weighted average of the MEA enthalpies (7.14 ± 0.42 kcal mol$^{-1}$)[31] for Xe adsorption on Na−MOR (Si/Al = 39.5).

**Insights from the Process Capacities of Na−Mordenite and H−Mordenite.** The process capacities are converted into accessible adsorbent surface areas (using the excluded molecular areas[12]) and pore volumes (using the calculated molar volumes, *MVL*[12]). Different literature reports give adsorbate molar volumes (used for molecular volume) and molecular areas that vary considerably. Generally, these molecular properties have been estimated from bulk properties, but many assumptions are required. The calculation of these properties eliminates the need to assume spherical symmetry of the adsorbate and a molecular packing in the structure.[12] Molecular properties, calculated molar volumes (*MVL*), and excluded molecular areas were determined previously[12] for the adsorptives utilizing ZINDO,[32] a series of molecular electronic structure programs from the Quantum Theory Project at the University of Florida, and are presented in Table 1.

The calculated MEA capacities ($n_i$), accessible surface areas, and pore volumes for Na−MOR can be found in Tables 4 and 6 for H−MOR. In general, the total process capacities decrease as the size of the probe increases. The fact that both $N_2$ and CO, which are larger than $O_2$, yield a total accessible adsorbent surface area greater than that of $O_2$ is due to their electron donor properties and higher polarizability, which permit specific donor−acceptor interactions with the solid.

As expected, the pore volume of the small channel is significantly less than the volume of the large channel. This difference aids in the distinction between the types of interactions. For Na−MOR, the type 1 accessible surface areas for $N_2$ and CO are lower than their type 2 and type 3 accessible surface areas. The type 1 accessible surface areas for both $N_2$ and CO are identical within error, and the type 2 value is equal (within error) to the type 3 values for both $N_2$ and CO. This information indicates that both $N_2$ and CO have similar interactions with the small channel, and the volume of the small channel is a minor proportion of the total pore volume; i.e., the large channel is the majority of the structural pore volume (structural porosity volume of the solid). Since the larger probes are excluded from the small channel, they may be used to determine information only about the large channel and the aperture of the small channel and yield no information about the small channel directly.

## Conclusions

Adsorption isotherms for eleven adsorptives were measured at multiple temperatures above their critical temperatures with the zeolite Na−mordenite and five representative adsorptives with H−mordenite. The multiple equilibrium analysis method (MEA), which fits the adsorption isotherms simultaneously to a minimum number of processes (Tables 3 and 5), provides process capacities, accessible surface areas, and pore volumes (Tables 4 and 6) and enthalpies and entropies of adsorption for each process (Tables 7 and 8). The adsorption process contains a narrow distribution of the same thermodynamic interaction parameters (within experimental error) and groups them together in describing the adsorption process (an interaction type). Mordenite was selected for study because it contains two channels with very different, fixed dimensions. The examination of Na−MOR and H−MOR has provided insights into the very complex energetics of adsorbate−adsorbent interactions. Unlike amorphous adsorbents, where for the first process an adsorptive can select pores of similar size from the distribution available, the first adsorption process that occurs in materials with uniform, fixed dimensions may not involve a pore of comparable size. This difference leads to the type designation terminology, used to indicate the degree of matching of adsorptive and pore dimensions.

Reversals in the magnitude of the enthalpy of adsorption ($-\Delta H_i$) and equilibrium constant ($K_i$) are found for the processes corresponding to adsorption of the larger adsorbates in the large channel of Na−MOR and H−MOR. The larger adsorbates studied did not exhibit any type 1 interactions with Na−MOR or H−MOR. The first process of the larger adsorbates has the larger $K$ and less negative enthalpy, indicating a type 3 interaction for the first process and a type 2 interaction for the second process. The entropy−enthalpy plots show that the type designation for the first process of $C_2H_6$ and $SF_6$ is type 2 and the second process is type 3 (Figure 8). A wide variety of probe molecules have been studied on carbonaceous adsorbents, and none show this reversal. In contrast to zeolites, the pores of the carbonaceous A-572 consist of parallel sheets or planes with localized graphitic domains. The adsorbate−adsorbent interactions occur along the surfaces of these planes, and a large adsorbate is less constrained in a slit-shaped pore than it is in a cylindrical pore. Reversals in $K_i$ and $\Delta H_i$ can be expected for some adsorbates in cylindrical-shaped pores.

The process capacities that result from MEA are as significant as the thermodynamic data. Using calculated molar volumes (*MVL*), one can calculate the accessible pore volume for an adsorbate. When adsorptive dimensions match pore dimensions, structural pore volumes result. A comparison of these volumes with those from standard $N_2$ porosimetry shows important

(28) The ratio of the MEA process 2 capacity to the total capacity is $0.37 \pm 0.1 = (0.93 \pm 0.09 \text{ mmol}/(0.93 \pm 0.09 \text{ mmol} + 1.57 \pm 0.01 \text{ mmol}))$.

(29) The ratio of the "side-pocket site" capacity (per unit cell) to the total "site" capacity (per unit cell) is 0.25 = (2 molecules/(2 molecules + 6 molecules)).[26]

(30) Ohgushi, T.; Yokoyama, H. *J. Chem. Soc., Faraday Trans.* **1992**, *88*, 3095−3099.

(31) $-\Delta H_{\text{weighted MEA}} = (7.14 \pm 0.42 \text{ kcal mol}^{-1}) = (n_1/n_{\text{tot}})(-\Delta H_1) + (n_2/n_{\text{tot}})(-\Delta H_2) = (0.627 \pm 0.013)(7.82 \pm 0.26) + (0.373 \pm 0.022)(5.995 \pm 0.067)$; $n_1/n_{\text{tot}} = 0.627 \pm 0.013 = (1.547 \pm 0.009 \text{ mmol})/(2.467 \pm 0.051 \text{ mmol})$; $n_2/n_{\text{tot}} = 0.373 \pm 0.022 = (0.92 \pm 0.05 \text{ mmol})/(2.467 \pm 0.051 \text{ mmol})$; $n_{\text{tot}} = n_1 + n_2 = 2.467 \pm 0.051 \text{ mmol} = (1.547 \pm 0.009) + (0.92 \pm 0.05)$.

(32) Zerner, M. C.; et al. ZINDO, Department of Chemistry, University of Florida, Gainesville, FL 32611. Zerner, M. C. *Reviews of Computational Chemistry*; VCH Publishing: New York, 1991; Vol. 2, pp 313−366.

differences. For measurements above the adsorptive critical temperature, monolayer coverage is expected, and conversion of the MEA process capacities (with excluded molecular areas) provides probe-dependent, accessible surface areas. Significant differences result between the values obtained in this manner and those from BET on microporous solids.

The larger equilibrium constants obtained for H−MOR compared to Na−MOR (Tables 5 and 3) indicate that H−MOR has a larger affinity for adsorbing the molecules studied due to the stronger interactions induced by the proton of H−MOR. The MEA description of adsorption provides a rational explanation of adsorbent differences using thermodynamic parameters and probe-dependent adsorbent capacities. The MEA method produces insight and a useful overall characterization of gas−solid interactions.

**Acknowledgment.** The authors would like to recognize the late Dr. Russell S. Drago for his insights and guidance in this project before his passing. The authors acknowledge very helpful discussions with Dr. Willis B. Person. The authors also acknowledge the assistance of Dr. Michael J. Scott and Dr. Michael C. Zerner. The Environmental Protection Agency (EPA), the National Science Foundation (NSF CHE-9726689), and the U.S. Army Edgewood Research and Development Center (ERDEC) provided financial support for this project. Computational time for the calculated molecular and molar properties included in Table 1 was supported by the Office of Naval Research (ONR) and an IBM SUR Grant at the J.C. Slater Computing Laboratory at the Quantum Theory Project of the University of Florida. Micromeritics Inc. offered technical assistance for the ASAP 2000 gas analyzer, and Mr. Todd A. Prox, Machine Shop Supervisor of the University of Florida Technical Services, assisted with the maintenance of the ASAP 2000 gas analyzer. The authors also acknowledge the Engineering Research Center for Particle Science and Technology at the University of Florida for the use of the Perkin-Elmer Optima 3200 RL ICP spectrometer and Ms. Gretchen Potts for technical assistance.

JA984122R